Journal of
Materials Chemistry C

PAPER

View Article Online
View Journal

Cite this: DOI: 10.1039/c6tc01034b

The structure, chemistry and magnetic properties of $FePbBiO_4$

Benjamin P. de Laune,[a] Frank J. Berry,[a] Jose F. Marco,[b] Sarah L. Horswell[a] and Colin Greaves*[a]

Received 10th March 2016,
Accepted 4th May 2016

DOI: 10.1039/c6tc01034b

www.rsc.org/MaterialsC

The compound $FePbBiO_4$ has been synthesised and has a tetragonal structure ($P4_2/mbc$, a = 8.48924(9) Å, c = 6.10597(8) Å) that is closely related to $FeSb_2O_4$. It provides the first example of a compound with this structure that (a) contains only trivalent ions (here Fe^{3+}) within the chains of edge-linked octahedra and (b) accommodates Bi^{3+} in the walls of the channels formed between the chains of octahedra. $FePbBiO_4$ orders antiferromagnetically with a Néel temperature of 24 K; neutron diffraction reveals A-type magnetic order with moments oriented perpendicular to [001]. The magnetic moment of Fe^{3+} at 4 K is 3.74(6) μ_B, slightly lower than that commonly observed for this cation in well-ordered magnetic oxides.

1 Introduction

The mineral schafarzikite, $FeSb_2O_4$, has been reported to be tetragonal ($P4_2/mbc$, a = 8.62 Å and c = 5.91 Å)[1] with one-dimensional features: chains of edge-linked FeO_6 octahedra are aligned along [001] and enclose parallel channels. This is illustrated in Fig. 1 for the detailed structure of the new compound reported here, $FePbBiO_4$ (or $Fe(PbBi)_2O_4$), where one Pb^{2+} and one Bi^{3+} ion have replaced two Sb^{3+} ions. In $FeSb_2O_4$, therefore, Sb^{3+} ions link the FeO_6 octahedra *via* their apical (O1) and equatorial (O2) ligands and form SbO_3 trigonal pyramids. The Sb^{3+} lone pairs (e) are directed into the channels and provide pseudo-tetrahedral SbO_3e coordination. Strong intrachain magnetic exchange (primarily direct orbital overlap between adjacent Fe^{2+} ions) results in A-type magnetic order (Fig. 2a) below the Néel temperature, T_N = 46 K.[2,3]

Related MSb_2O_4 materials (M = magnetic transition metal) are known for M = Mn, Co, Ni, Cu and Zn.[4–8] All order magnetically at low temperatures except for $CuSb_2O_4$, which appears to show no long range order above 2 K,[9] and $ZnSb_2O_4$, which is diamagnetic. Whereas the phases with M = Mn, Fe display predominantly A-type magnetic order (Fig. 2a), the M = Co, Ni phases are C-type antiferromagnets (Fig. 2b).[1,10,11] It has been suggested that the nature of the direct exchange within the chains – size of cation, M–M separation distance and occupancy of the t_{2g} orbitals – is responsible for the change in magnetic order.[11,12] The 90° M–O–M intrachain exchange is expected to be ferromagnetic but weak for all ions in the series Mn···Ni. However, Mn^{2+} and Fe^{2+} experience strong direct antiferromagnetic exchange because the t_{2g} orbitals are relatively diffuse; this allows overlap of orbitals on adjacent cation sites to give an antiferromagnetic groundstate. Across the series from Mn to Ni, the d-orbitals contract and the t_{2g} orbitals fill up both of which weaken the direct exchange such that intrachain ferromagnetic order occurs to give, overall, C-type order. In confirmation of these basic principles, the change in magnetic order for the series $Fe_xCo_{1-x}Sb_2O_4$ and $Mn_xCo_{1-x}Sb_2O_4$, $0 \leq x \leq 1$ has recently been reported and shows a gradual change from A-type to C-type as x decreases.[12]

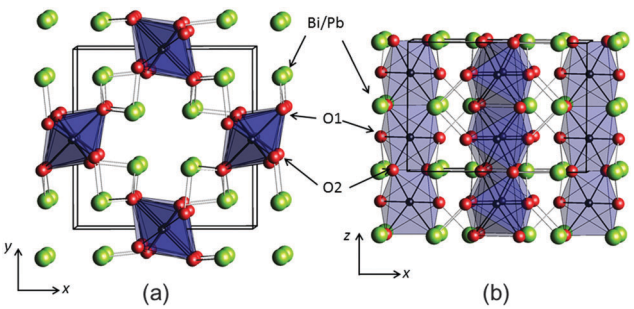

Fig. 1 The structure of $FePbBiO_4$ structure viewed (a) along [001] and (b) approximately along [010]. Fe – black within blue octahedra, Pb/Bi – large green spheres, O – red spheres (O1 apical and O2 equatorial).

Attempts to functionalise some materials by creating mixed M^{2+}/M^{3+} oxidation states have been reported *via* substitution of Pb^{2+} for Sb^{3+} for M = Mn, Fe and Co.[11,13,14] However, only for M = Fe is oxidation of the transition metal favoured over oxidation of Sb^{3+} to Sb^{5+}.[13] Even for this system, $FeSb_{2-x}Pb_xO_4$, pure crystalline products were obtained only for $x \leq 0.7$ and no phase containing 100% Fe^{3+} (requiring equal amounts of +2 and +3 charged lone pair cations) has been reported.

[a] School of Chemistry, University of Birmingham, Birmingham B15 2TT, UK. E-mail: c.greaves@bham.ac.uk
[b] Instituto de Quimica-Fisica "Rocasolano", CSIC, Serrano 119, 28006 Madrid, Spain

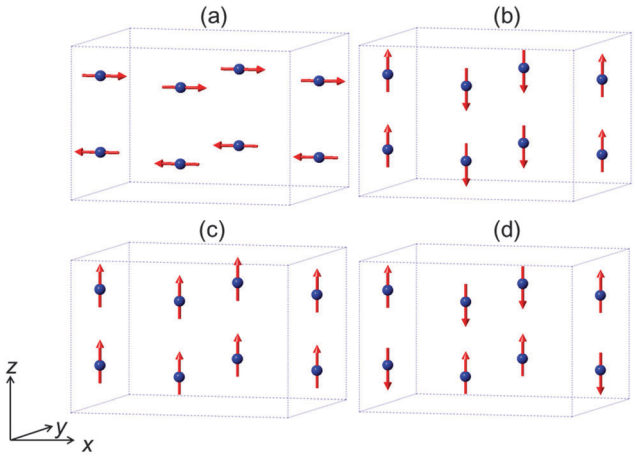

Fig. 2 The four possible collinear spin alignments generating the basic observed magnetic structures for MSb_2O_4 phases: (a) A-type, (b) C-type, (c) F-type and (d) G-type.

The magnetic properties of such a material are of interest because the direct exchange would be expected to be weaker than in the Fe^{2+} compound, $FeSb_2O_4$, such that the resultant magnetic order is not simple to predict. It is also strange that no schafarzikite-type phase containing Bi^{3+} ions has been reported since the ionic radius of Bi^{3+} (1.03 Å) is intermediate between those of Pb^{2+} (1.19 Å) and Sb^{3+} (0.76 Å); these data are for 6-coordinate ions since data are not given for 3-coordination.[15] In the present study, we examined the use of the similarly sized cations Pb^{2+} and Bi^{3+} and we report the successful synthesis, structure, magnetic properties and chemistry of the resultant product $FePbBiO_4$: the first schafarzikite compound to contain only +3 cations within the chains of octahedra and the first to contain Bi^{3+} cations.

2 Experimental

A polycrystalline sample of $FePbBiO_4$ was synthesised by heating an intimate mixture of pre-dried Fe_2O_3 (99%, Aldrich), PbO (99.9%, Aldrich) and Bi_2O_3 (99.9%, Aldrich) in the appropriate stoichiometric amounts. The mixture was heated in air for two periods of 7 h at 650 °C in an alumina boat.

X-Ray powder diffraction (XRPD) data were collected on a Bruker D8 diffractometer (PSD: Lynxeye, Cu-$K_{\alpha 1}$, Ge monochromator) in planar transmission mode. Neutron powder diffraction (NPD) data were collected on diffractometer D2B, ILL, Grenoble at temperatures of 300, 20, 16 and 4 K. The wavelength was calibrated using XRPD refinement data on the same sample to give λ = 1.5923 Å. The ILL data used for the refinements were extracted from only the centre of the detectors to provide greater peak resolution.

A ^{57}Fe Mössbauer spectrum was recorded at 298 K with a constant acceleration spectrometer in transmission geometry using a *ca.* 400 MBq ^{57}Co/Rh source. To avoid the effects of excessive absorption by the presence of Pb and Bi, a sample enriched to 10% ^{57}Fe was synthesised. The drive velocity was calibrated with the ^{57}Co/Rh source and a natural iron foil. The chemical isomer shift data are reported relative to that of metallic iron at 298 K.

The Rietveld method[16] was used to refine the nuclear and magnetic structures of $FePbBiO_4$ with the aid of the general structures analysis system (GSAS)[17] and EXPGUI interface.[18] Background intensity was modelled using a shifted Chebyschev polynomial with 25 terms, while peak shapes were modelled using a pseudo-Voigt function. Isotropic displacement parameters were assigned to Fe^{3+} and the equatorial O2, but anisotropic parameters were used for Pb^{2+}/Bi^{3+} and the apical O1. The magnetic structure was modelled using a second unit cell ($P1$) containing only magnetic cations, with appropriate constraints applied to the magnetic moments to conform to a given model. The unit cell dimensions of the magnetic phase were constrained to those of the nuclear unit cell.

Magnetic susceptibility data were acquired using a Quantum Design MPMS SQUID under field cooled (FC) and zero field cooled (ZFC) conditions with an applied field of 100 Oe. No corrections for diamagnetism were applied since they are too small to provide a significant effect. A cooling and heating rate of 10 K min^{-1} was used, with measurements taken in 'Sweep' mode. The polycrystalline sample (~70 mg) was contained in a gelatin capsule, within a plastic straw.

3 Results and discussion

3.1 Crystal structure

The synthesised $FePbBiO_4$ was dark brown and stable in air up to the melting point at ~700 °C. The ambient temperature Mössbauer spectrum, Fig. 3, shows a single Fe^{3+} doublet with a chemical isomer shift, δ, of 0.39 mm s^{-1} and quadrupole splitting, Δ, of 0.59 mm s^{-1}. These values are typical of octahedral Fe^{3+} and confirm that the synthesis yields a product for which 100% of the Fe is present as Fe^{3+}. XRPD data revealed the product to be single phase with a tetragonal, $P4_2/mbc$, structure which is indicative of the schafarzikite structure. The unit cell parameters determined from Rietveld refinement against X-ray data were subsequently used to calibrate the NPD data, against which the structure was refined. The refined structural parameters are given in Table 1 for data obtained at ambient temperature and 4 K. The relevant diffraction profiles corresponding to the refinement based on ambient temperature

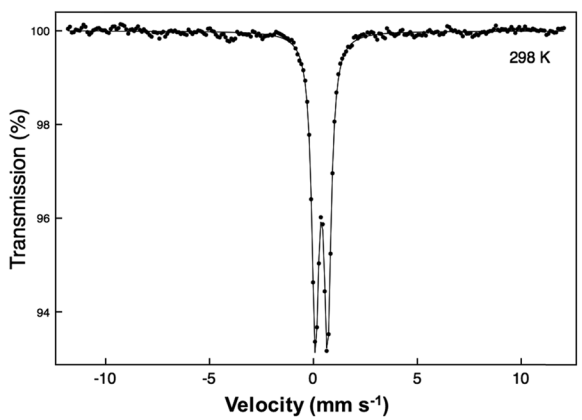

Fig. 3 The ambient temperature ^{57}Fe Mössbauer spectrum of $FePbBiO_4$.

Table 1 Refined structural parameters from NPD data from $FePbBiO_4$ at 300 K and 4 K (the latter are given in italics)

Atom	Site	x	y	z	U_{iso} (or U_{eq}) × 100/Å^2
Fe	*4d*	0.0	0.5	0.25	0.91(3)
					0.58(4)
Pb/Bi	*8h*	0.1541(1)	0.1570(1)	0.0	1.65[a]
		0.1547(2)	*0.1558(2)*	*0.0*	*1.13*[a]
O1	*8g*	0.6686(1)	0.1686(1)	0.25	2.74[a]
		0.6687(2)	*0.1687(2)*	*0.25*	*1.86*[a]
O2	*8h*	0.0930(2)	0.6303(2)	0.0	1.34(3)
		0.0916(3)	*0.6313(3)*	*0.0*	*0.70(5)*

Atom	U_{11}	U_{22}	U_{33}	U_{12}	U_{13}	U_{23}
Pb/Bi	1.27(6)	2.10(6)	1.59(4)	0.21(4)	0.0	0.0
	0.68(9)	*1.58(10)*	*1.13(8)*	*0.23(6)*	*0.0*	*0.0*
O1	3.54(6)	3.54(6)	1.14(6)	−2.40(7)	−0.99(5)	0.99(5)
	2.52(9)	*2.52(9)*	*0.52(11)*	*−1.51(12)*	*−0.66(10)*	*−0.66(5)*

$P4_2/mbc$: a = 8.48925(9) (*8.4725(2)*) Å, c = 6.10597(8) (*6.1004(2)*) Å, volume = 440.04(1) (437.90(3)) Å^3. R_{wp} = 0.036 (*0.056*); χ^2 = 4.19 (*8.98*). [a] Anisotropic displacement parameters (all × 100/Å^2) are given.

data are shown in Fig. 4. The Bi and Pb ions were found to be randomly distributed on the channel wall site; it was found that this position and the apical O1 site had higher than expected isotropic displacement parameters (IDPs). Allowing anisotropy resulted in strongly anisotropic parameters (ADPs) as shown in Table 1. These values are attributed to the presence of both Pb^{2+} and Bi^{3+}: the charge and size differences, as discussed in the Introduction, result in local displacements of the cations and the O1 ions, to which they are bonded. The effects of the ADPs are highlighted in Fig. 5, which focuses on this region of the structure. The local displacements of Pb/Bi towards or away from the bonded O1 are indicated, and O1 moves in a perpendicular direction so that the Fe–O1 bond distance will not change significantly. The displacements allow optimisation of the bonding requirements according to whether Pb^{2+} or Bi^{3+} is bonded to a particular O1 site. Table 2 gives important bond distances and angles and also provides bond valence sums (BVS)[19] for the cations and the full structure is shown in Fig. 1.

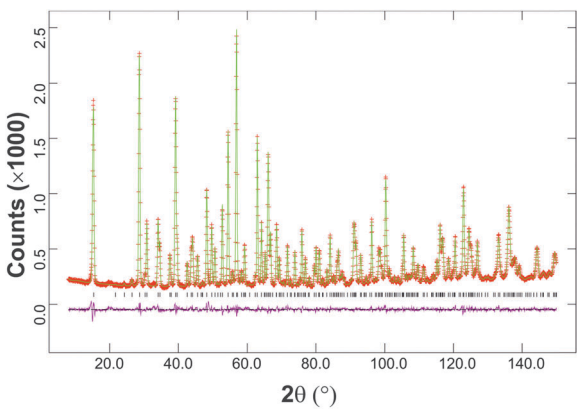

Fig. 4 Fitted neutron powder diffraction profiles at 300 K showing observed data (red crosses), calculated (green line) and difference (purple line). Reflection markers are shown below the diffraction profiles.

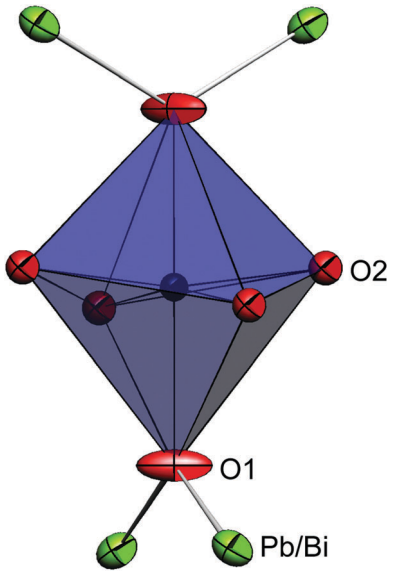

Fig. 5 Ion displacements represented by contours enclosing 70% of the neutron scattering.

Table 2 Significant bond distances, bond valence sums (BVS) and angles at 300 K

Bond		Distance/Å	BVS	
Fe	–O1	2.024(1) [×2]	2.83	
	–O2	2.0435(9) [×4]		
Pb/Bi	–O1	2.1298(10)...[×2]	Pb^{2+} 2.79	Bi^{3+} 2.65
	–O2	2.159(2)		

Bond	Angle/°
O1–Fe–O1	180.0(0)
O1–Fe–O2	83.71(4) [×4]
	96.29(4) [×4]
O2–Fe–O2	83.34(5) [×2]
	98.05(5) [×2]
O1–Pb/Bi–O1	91.57(5)
	90.89(5) [×2]

The unit cell volume (440.0 Å^3, Table 1) is similar to that of $FeSb_2O_4$ (439.5 Å^3),[13] which reflects a balance in the effects of replacing Fe^{2+} with the smaller Fe^{3+} whilst, at the same time, substituting the larger Pb^{2+}/Bi^{3+} combination for Sb^{3+}. However, a contraction occurs along a and an expansion along c (for $FeSb_2O_4$: a = 8.6157(1) Å, c = 5.9207(1) Å).[13] This effect is universally seen when oxidation occurs at the octahedral intra-chain cation owing to enhanced electrostatic repulsions across the common edges of the linked octahedra.

Although the BVS for Fe^{3+} is close to that expected (Table 2), the determined Pb/Bi site provides a highly "overbonded" location for Pb^{2+} whereas Bi^{3+} would be somewhat "underbonded". However, these values are to be expected since they are determined from the average Pb/Bi and O ionic positions and are consistent with the ADP values, which represent an attempt to model the

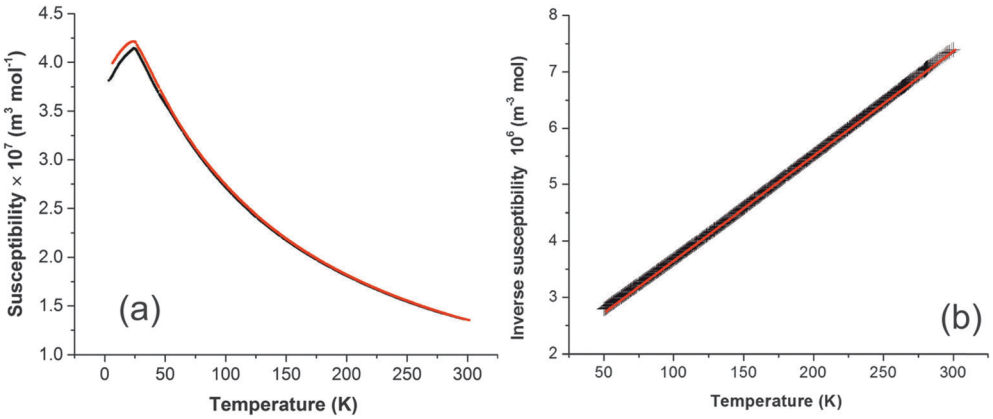

Fig. 6 (a) Plot of magnetic susceptibility against temperature for $FePbBiO_4$ (FC data red, ZFC data black). (b) Plot of inverse susceptibility against temperature (data are black, linear fit is red).

distribution of the average scattering from the O, Pb and Bi nuclei. Because of the electrostatic repulsion between Fe^{3+} cations within the chains of edge-linked octahedra along [001], the octahedra are extended in this direction; this provides O2–Fe–O2 equatorial angles of 83.34(5)° (where the angle bisector is parallel to [001]) and 98.05(5)° (where the bisector is perpendicular to [001]).

3.2 Magnetic properties

Magnetic susceptibility (χ) data for $FePbBiO_4$ are shown in Fig. 6a and suggest a simple paramagnetic-antiferromagnetic transition with a Néel temperature of 24 K; a small divergence between the FC and ZFC susceptibilities below T_N is possibly due to a slight canting of the moments. Fig. 6b shows the variation of $1/\chi$ with temperature, which is exactly linear such that it is difficult to differentiate the data points and the least squares fit; the material therefore strictly obeys the Curie–Weiss law: the slope corresponds to an effective moment of $\mu_{eff} = 5.870(1)\ \mu_B$ and the intercept on the temperature axis gives the Weiss constant, $\theta = -97(1)$ K. As expected for a d^5 high spin cation, for which there is zero orbital contribution to the magnetic moment, the moment is in excellent agreement with the spin-only moment of 5.92 μ_B. As is usual for materials with this structure, $-\theta$ is significantly greater than T_N; this may be rationalised since θ will reflect the average exchange energy (intrachain and interchain) at temperatures above T_N, whereas T_N is determined largely by the weaker interchain exchange interactions.[12]

The low temperature magnetic order was explored by collecting NPD data sets at 4 K, 16 K and 20 K. The nuclear structural parameters at 4 K are given in Table 1 and show no major changes compared with those at 300 K. Symmetry allows a range of magnetically ordered structures. Fig. 2 shows the basic types of magnetic order that have been observed for MSb_2O_4 materials, but the actual order in these materials can be complex, with contributions from more than one of the types of order shown in Fig. 2.[12] A separate magnetic phase with $P1$ symmetry was therefore used in the low temperature refinements to allow complete flexibility. The principal order observed was found to be A-type with moments aligned along [100], A_x, or the equivalent A_y. Although a small C_z component was observed for the largest overall moment (at the lowest temperature, 4 K), at higher temperatures no significant evidence for this was apparent. The refined moments are given in Table 3, where μ_x gives the A-type moment and μ_z the C-type component. The mixture of A_x and C_z components at 4 K corresponds to a small rotation of the moments by 6.3(8)° away from the x-axis towards the z-axis. The NPD profiles at 300 K and 4 K are compared in Fig. 7 for $2\theta < 40°$, where strong magnetic scattering is observed.

The NPD data show that $FePbBiO_4$ and $FeSb_2O_4$ display the same principal magnetic order: A_x-type with antiferromagnetic order within the chains of FeO_6 octahedra. However, the overall exchange interactions appear to be weaker for $FePbBiO_4$, since T_N (24 K) is significantly lower than that for $FeSb_2O_4$, 46 K.[2,3] The $Fe^{3+}\cdots Fe^{3+}$ direct exchange is probably weaker in $FePbBiO_4$ because of the more contracted d-orbitals of Fe^{3+}. It is also likely that the extended interchain covalent exchange pathway (Fe–O–Pb/Bi–O–Fe) is reduced in energy. Given the increased size of Co^{2+} compared with Fe^{3+}, it is a little surprising that $CoSb_2O_4$ displays C-type order[11] (with ferromagnetic order within a given chain of octahedra) whereas $FePbBiO_4$ is A-type, which is normally associated with strong direct exchange. This feature can be rationalised by the difference in electron configurations within the t_{2g} orbitals participating in the direct exchange: $(t_{2g})^5$ and $(t_{2g})^3$, respectively. In contrast to Fe^{3+}, where all t_{2g}–t_{2g} overlaps will result in antiferromagnetic exchange, for Co^{2+} both antiferromagnetic and ferromagnetic exchange interactions are present depending on the electron occupancy of the overlapping orbitals; this will reduce the overall tendency for antiferromagnetic chain order.

The refined magnetic moment at 4 K, 3.74(6) μ_B, is lower than the ideal value of 5 μ_B for Fe^{3+}. However, the value is

Table 3 Magnetic data for $FePbBiO_4$ from NPD refinements

Temperature/K	μ_x/μ_B	μ_z/μ_B	μ_{total}/μ_B
4	3.72(5)	0.41(7)	3.74(6)
16	3.17(6)	0	3.17(6)
20	2.70(7)	0	2.70(7)

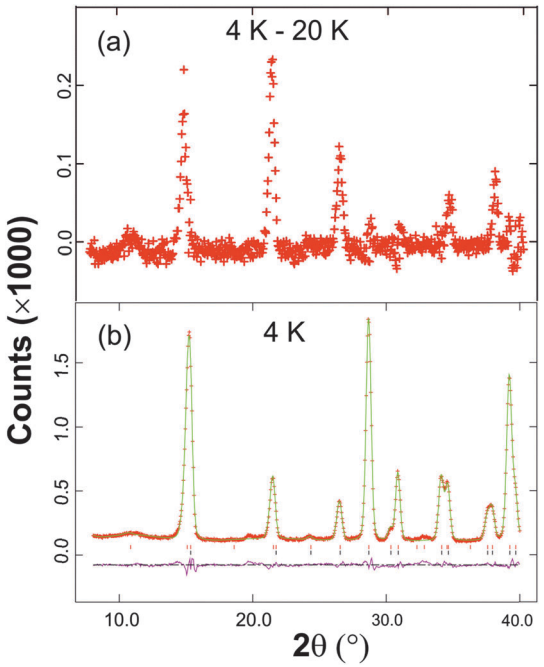

Fig. 7 (a) The difference between the observed NPD profiles at 4 K and 20 K demonstrating the areas of large magnetic scattering. (b) Fitted neutron powder diffraction profiles at 4 K for $2\theta < 40$ K: observed data (red crosses), calculated (green line) and difference (purple line). Reflection markers for the magnetic and nuclear unit cells are shown in red and black, respectively.

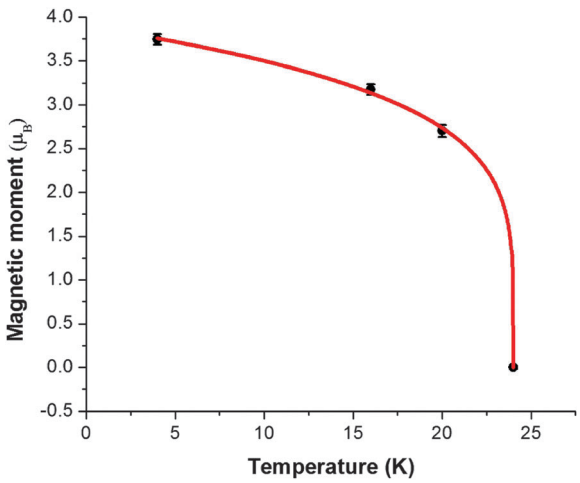

Fig. 8 Variation of ordered magnetic moment (●) with temperature fitted to a Brillouin function (red line).

similar to values normally seen for Fe^{3+} compounds, and the reduced moment is caused by zero-point quantum mechanical effects and ligand-to-metal electron transfer inherent to covalence within the Fe–O bonds.

The overall magnetic moments are plotted against temperature in Fig. 8. The Néel temperature from the susceptibility measurements has been included and the resulting four data points fit well to the Brillouin function $\mu = \mu_0\left(1 - \frac{T}{T_N}\right)^{\beta}$ where the Néel temperature, T_N, is fixed at 24 K, μ_0 is the zero-point moment and β is an exponent that is linked to the nature of the transition. In this case, fitting the data results in the parameters: μ_0, = 3.89(4) μ_β, and β = 0.20(1). Although lower than that normally found for magnetic order in isotropic materials (for which β is usually *ca.* 0.3), β is typical for low dimensional systems and is similar to the value of 0.18 reported for $FeSb_2O_4$.[3]

4 Conclusions

Tetragonal $FePbBiO_4$ has been synthesised and its unit cell shows a contraction along *a* and an expansion along *c* compared with that of $FeSb_2O_4$. These changes are the result of enhanced electrostatic repulsion between the Fe^{3+} cations within the chains of octahedra oriented along [001]. The Bi^{3+} and Pb^{2+} ions are randomly distributed on the sites which form the walls of the channels within the structure, and their bonding preferences result in small differences to their ionic positions; these are reflected in the atomic ADP values. Below the Néel temperature (24 K), $FePbBiO_4$ displays A-type antiferromagnetic order with moments perpendicular to [001]. The magnetic moment of Fe^{3+} at 4 K is 3.74(6) μ_B, slightly lower than expected for this cation in well-ordered magnetic oxides.

Acknowledgements

We thank EPSRC for financial support of this research (EP/L014114/1) and EPSRC, EU and ILL for the provision of NPD facilities. We are grateful to Dr Emma Suard for assistance in collecting the NPD data and Dr Martin Lees for the use of a SQUID at the Department of Physics, University of Warwick. The X-ray diffractometers used in this research were obtained through Birmingham Science City: Creating and Characterising Next Generation Advanced Materials (West Midlands Centre for Advanced Materials Project 1), with support from Advantage West Midlands (AWM) and part funded by the European Regional Development Fund (ERDF). Data associated with the results shown in this paper are accessible from the University of Birmingham Archive: http://epapers.bham.ac.uk/2162/.

References

1 J. A. Gonzalo, D. E. Cox and G. Shirane, *Phys. Rev.*, 1966, **147**, 415.
2 F. Varret, P. Imbert, A. Gerard and F. Hartmann-Boutron, *Solid State Commun.*, 1968, **6**, 889.
3 R. Chater, J. R. Gavarri and A. W. Hewat, *J. Solid State Chem.*, 1985, **60**, 78.
4 G. Tammann, *Z. Anorg. Allg. Chem.*, 1925, **149**, 21.
5 E. Koyama, I. Nakai and K. Nagashima, *Nippon Kagaku Kaishi*, 1979, **6**, 793.
6 J. R. Gavarri, G. Calvarin and B. Chardon, *J. Solid State Chem.*, 1983, **47**, 132.
7 H. T. Witteveen, *Solid State Commun.*, 1971, **9**, 1971.
8 S. Ståhl, *Ark. Kern. Min. Geol.*, 1943, **17B**, 1.

9 M. T. Atanasova, A. M. Strydom, C. J. H. Schutte, L. C. Prinsloo and W. W. Focke, *J. Mater. Sci.*, 2014, **49**, 3497.
10 J. R. Gavarri and A. W. Hewat, *J. Solid State Chem.*, 1983, **49**, 14.
11 B. P. de Laune and C. Greaves, *J. Solid State Chem.*, 2012, **187**, 225.
12 J. Cumby, B. P. de Laune and C. Greaves, *J. Mater. Chem. C*, 2016, **4**, 201.
13 M. J. Whitaker, R. D. Bayliss, F. J. Berry and C. Greaves, *J. Mater. Chem.*, 2011, **21**, 14523.
14 A. M. Abakumov, M. G. Rozova, E. V. Antipov, J. Hadermann, G. Van Tendeloo, M. V. Lobanov, M. Greenblatt, M. Croft, E. V. Tsiper, A. Llobet, K. A. Lokshin and Y. S. Zhao, *Chem. Mater.*, 2005, **17**, 1123.
15 R. D. Shannon, *Acta Crystallogr., Sect. A: Cryst. Phys., Diffr., Theor. Gen. Crystallogr.*, 1976, **32**, 751.
16 H. M. Rietveld, *J. Appl. Crystallogr.*, 1969, **2**, 65.
17 A. C. Larson and R. B. Von Dreele, *General Structural Analysis System (GSAS)*, Los Alamos National Laboratory LAUR, 1994, pp. 86–748.
18 B. H. Toby, *J. Appl. Crystallogr.*, 2001, **34**, 210.
19 I. D. Brown and D. Altermatt, *Acta Crystallogr., Sect. B: Struct. Sci.*, 1985, **41**, 244.

